LBL-11572
Preprint

Lawrence Berkeley Laboratory
UNIVERSITY OF CALIFORNIA

Materials & Molecular
Research Division

Submitted to the Journal of the American Ceramic Society

QUANTITATIVE STUDIES OF THERMAL SHOCK IN CERAMICS BASED ON A NOVEL TEST TECHNIQUE

K.T. Faber, M.D. Huang, and A.G. Evans

May 1981

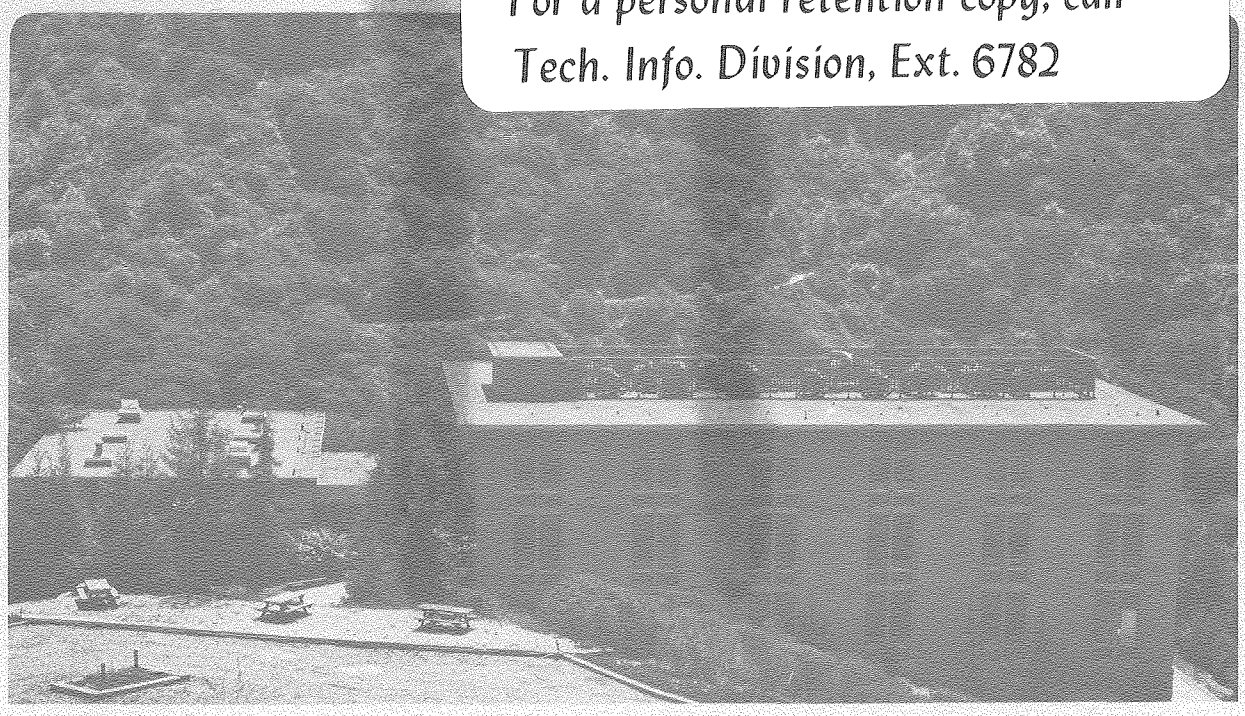

Prepared for the U.S. Department of Energy under Contract W-7405-ENG-48

DISCLAIMER

QUANTITATIVE STUDIES OF THERMAL SHOCK IN CERAMICS

BASED ON A NOVEL TEST TECHNIQUE

by

K. T. Faber[‡]

Alpha Silicon Carbide Division
The Carborundum Co.
Niagara Falls, N.Y. 14302

M. D. Huang

and

A. G. Evans

Materials and Molecular Research Division, Lawrence Berkeley Laboratory
and Department of Materials Science and Mineral
Engineering, University of California
Berkeley, CA 94720

This work was supported by the Director, Office of Energy Research, Office of Basic Energy Sciences, Materials Science Division of the U.S. Department of Energy under Contract No. W-7405-ENG-48.

[‡]Now at University of California, Berkeley.

ABSTRACT

A thermal shock test has been designed which permits the thermal fracture resistance and the mechanical strength of brittle materials to be quantitatively correlated. Thermal shock results for two materials, Al_2O_3 and SiC, have been accurately predicted from biaxial strength measurements and a transient thermal stress analysis (performed using a finite element method). General implications for the prediction of thermal shock resistance, with special reference to ceramic components, are discussed.

1. INTRODUCTION

Thermal transients are a ubiquitous source of fracture in ceramic components. A thorough comprehension of the variables that dictate thermal fracture are thus essential if the reliable performance of ceramics in fracture critical applications is to be achieved. A logical approach for evaluating the susceptibility of a ceramic component to failure during a thermal transient is based on a parity between thermal shock resistance and mechanical strength.* However, this approach has not been uniquely validated; in fact, certain observations on ceramics appear to be superficially inconsistent with the approach[1]. Two comparative studies have been conducted[2,3] that afford some confidence in the pertinence of the mechanical strength for thermal shock prediction. Manson and Smith[2] presented statistical relations between mechanical strength (measured in flexure) and thermal shock resistance, and demonstrated that the statistical shape parameters deduced from both thermal shock and flexural strength tests (performed on steatite) were similar. However, they did not attempt a prediction of the absolute thermal failure condition from their mechanical strength data. More recently, the thermal failure of a precracked polymer[3] has been predicted from independent measurements of the crack dimensions and the critical stress intensity factor, by employing a numerical thermal stress analysis. In this study, an approximate choice of the heat transfer coefficient was used to provide reasonable predictions of the failure condition. The intent of the present paper is to provide a fully quantitative prediction of thermal failure. This is achieved by developing a suitable thermal shock test and by devising a method for the accurate calibration

*The mechanical strength refers to the stress level when the stress intensity factor at the fracture initiating flaw attains the critical value, K_{Ic}.

of the heat transfer coefficient; a method which involves the conduct of failure tests on a model brittle material (e.g. Al_2O_3). The thermal failure of another ceramic material (SiC) is then predicted from mechanical strength data by adopting the previously calibrated heat transfer coefficient.

A quantitative, but simple thermal shock test for evaluating and comparing ceramic materials (especially those suitable for advanced application such as gas turbine engines, heat exchangers and solar collectors) is not presently available. A procedure commonly adopted for thermal shock evaluation is based upon a water quench test[4]; the results of which can be incorporated into established theories of fracture initiation and crack propagation[5]. Under the high heat transfer conditions that prevail during a water quench, heat transfer and size effects have, in most previous studies, been assumed to be of negligible importance. The peak thermal stress, $\hat{\sigma}$, has then been calculated by applying the simple equation;

$$\hat{\sigma} = \frac{E\alpha\ \Delta T}{1 - \nu} \qquad (1)$$

where E is Young's modulus, α is the coefficient of thermal expansion, ΔT is the temperature differential across the specimen and ν is Poisson's ratio. By setting the peak tension equal to the equivalent fracture stress of the material, an estimate of the maximum temperature differential, ΔT_c, that can be sustained by a material prior to severe strength degradation is then provided. However, the water quench test has several problems which limit its utility as a quantitative test for evaluating thermal shock resistance.

Firstly, it has recently been shown that the above relation is only

independent of sample size when the samples are extremely large[6]. Thus, ΔT_c shows a strong size dependence in many experiments, rendering material ranking somewhat questionable. Secondly, the heat transfer rates encountered in typical ceramic applications (cited above) are appreciably smaller than those enforced by a water quench. The magnitudes of the thermal stresses expected in these applications are thus smaller than anticipated by Eq.(1), and described by the general result:

$$\sigma = \left[\frac{E\alpha\ \Delta T}{1-\nu}\right] F\left(\frac{hr}{k}\right) G\left(\frac{kt}{c\rho r^2}\right) \qquad (2)$$

where h is the heat transfer coefficient, k is the thermal conductivity, c is the specific heat, ρ is the density and r is a specimen dimension; the quantity hr/k is known as the Biot modulus, $kt/c\rho r^2$ is the Fourier number and F and G are functions[7]. Hence, many more material parameters influence typical thermal shock failures than the elementary water quench test analysis admits. Thirdly, complex variations in the heat transfer coefficient with test conditions present appreciable interpretation difficulties. For example, in one study performed on a metal wire in water, h was found to vary by $>10^4$ between 20 and 400°C, due to boiling at the metal-water interface[8]. Although the heat transfer variability can be essentially eliminated by quenching into oil, edge and corner effects cause futher difficulties.[9]

A thermal shock resistance testing and evaluation procedure which alleviates the difficulties associated with variable and very high heat

transfer rates and edge effects is proposed in this paper. The rationale and the experimental procedure are firstly presented and discussed. A numerical stress analysis, essential to the detailed interpretation of the experimental results, is then described. Finally, some important implications for fracture prediction under thermal transients are discussed.

2. EXPERIMENTAL

2.1 Rationale

The mechanical fracture of a ceramic exhibits appreciable statistical variability. The statistical nature of the fracture also results in a fracture criticality that depends upon the stressed volume and the stress state. These statistically derived effects pose considerable limitations upon the direct comparison of mechanical fracture and thermal shock. This difficulty is alleviated if the comparisons are conducted on samples with controlled pre-cracks, which extend to failure with minimal statistical variability. The principal experimental results are those obtained on pre-cracked specimens. The pre-cracks are introduced at the locations of peak tension, to provide a basis for subsequent comparisons of normally prepared surfaces at the location of maximum fracture probability.

The experiments are designed to provide a comparison of the mechanical strength and the critical temperature for thermal fracture initiation, at a prescribed location and under equivalent stress states (equi-biaxial tension). This is achieved by employing disc samples, in which the edge stresses (and hence, undesirable edge initiated failure) can be essentially eliminated. The mechanical tests are conducted in a biaxial flexure mode; while the thermal tests utilize a disc at uniform initial temperature, cooled by a fluid jet impinging upon the disc center.

2.2 Procedures

Two materials were selected for the thermal shock study: a 99% dense sintered α-SiC (~ 7 μm grain size) and a fully dense slip cast Al_2O_3 (~ 15 μm grain size). The samples, 5 cm diameter discs, 0.25 cm thick, were ground and polished on one surface. Subsequently, the centers of the polished faces were precracked using a Knoop indenter with loads of 15 to 33N. Residual stresses caused by the indentation process were removed by fine grinding.[10]

Each sample (both precracked and non-precracked) was individually tested in the thermal stress apparatus shown in Fig. 1. The sample was mounted horizontally on fibrous insulation (with two thermocouples placed against the surface of the specimen) and heated in a $MoSi_2$ resistance tube furnace. The sample was allowed to equilibrate, at which time is was subjected to a rapid temperature change, through the use of high velocity air. The air was channeled onto the disc center, using a 0.32 cm diameter silica tube, at a velocity of ~ 100 ms^{-1}. After the quench, the sample was examined for crack extension. If the crack did not extend, the temperature differential between the sample and the air jet was incrementally enhanced until crack extension was detected. This critical temperature differential, ΔT_c, was recorded. Fractographic analysis was performed to insure that fracture originated at the precracks in the indented samples. Typical specimens failed by thermal shock are shown in Fig. 2.

Identical samples were tested in biaxial flexure at room temperature using the apparatus designed by Wachtman et al.[11]. A 5 cm disc was

supported on three equally spaced balls (concentric with the load) and loaded with a flat piston at the rate of $\sim 2 MPa s^{-1}$.

3. RESULTS

The variations in the critical imposed temperature differential with indent load obtained for Al_2O_3 are shown in Fig. 3. The results were obtained by employing successive 10°C temperature increments, prior to failure. Fracture in the precracked specimens occurred within a relatively narrow ΔT range for each precrack size. The critical temperature differential increased as the precrack size diminished, ranging between 480° and 580°C. The specimens with as-machined surfaces failed over a wider range of temperature: a phenomenon related to the flaw size distribution. The approximate failure times (obtained from the time when the temperature at the lower thermocouple registered a rapid decrease) were ~ 5 s.

Results for sintered α-SiC were more difficult to obtain, because this material is subject to time dependent strengthening (by oxidation or by surface diffusion) within the temperature range required to induce thermal fracture, $\gtrsim$ 1100°C. It was elected, therefore, to obtain upper and lower bound values for ΔT_c by performing only a single thermal shock test on each precracked specimen (in contrast to the sequential testing employed with Al_2O_3). Firstly, a preliminary upper bound ΔT_c was established for each specific precrack size, by inducing thermal failure. Subsequent tests on specimens with the same precrack size were then performed at sequentially lower temperatures. The lowest temperature at which failure occurred was designated the upper bound, while the highest survival temperature was denoted the lower bound. The results obtained using this procedure are plotted in Fig. 3. It is

noted that samples without precracks could not be thermally shocked within the temperature limitations of the present system (~1500°C).

The biaxial flexure data for both materials are plotted as a function of the indentation load in Fig. 4. The theoretical slope[12] of -1/3 is superimposed to emphasize the trend. It is noted that SiC exhibits lower indentation strengths than Al_2O_3; a trend that probably reflects the fracture toughness characteristics of the two materials[12].

4. STRESS ANALYSIS

The thermal stresses that develop within the disc following impingement of the air jet were determined using axisymmetric finite element schemes. The temperature distributions were established by direct application of the program DOT[13]. The temperatures were then used to ascertain the thermal stress, by an adaptation of the program SOLSAP.[14]

The calculations were conducted by allowing heat transfer through the upper surface of the disc, to the air stream. Radiation from the lower surface of the disc into the cooled regions was also permitted. The heat transfer coefficient was assumed to be uniform over the diameter of the air jet, with a magnitude proportional to that expected for a fluid stream flowing against a thin plate;[15]

$$h = \lambda \frac{k_f}{d} \left(\frac{v_\infty d}{\eta_f} \right)^{0.7} P^{1/3} \qquad (3)$$

where k_f and η_f are the thermal conductivity and kinematic viscosity of the fluid at the film temperature, d is the jet diameter, v_∞ is the fluid velocity and P is the Prandtl number; λ is a proportionality constant, to be determined by a calibration procedure, described below.

Heat transfer was also considered to occur as a consequence of the jetting of the fluid over the surface. The heat transfer coefficient for boundary layer flow over a flat surface was selected,[15] and

allowed to diminish inversely with distance from the jet, to account for flow attenuation. However, preliminary calculations indicated that reasonable choices for this heat flow exerted a relatively minor influence on the thermal stress developed at the disc center (the location of present interest).

Four axisymmetric element groups were employed in the study: an interior two dimensional element (group 1), a surface convection element with constant heat transfer (group 2), a surface convection element with h inversely proportional to radial distance (group 3) and a uniform radiation element (group 4). The assignment of these elements is illustrated in Fig. 5. Four different meshes were selected (Fig. 6) in order to ascertain the influence of the mesh definition and to establish convergence conditions. It was firstly established that consistent results emerged provided that the mesh distribution was relatively uniform both in the central region (of high heat transfer) and across the adjacent discontinuity in h. Thereafter, it was determined that a grid with 216 elements (grid (c) in Fig. 6) was the preferred choice for subsequent analysis. This grid yielded temperature distributions within 1% and stresses within 6% of those calculated with the finest grid (559 elements): an accuracy deemed sufficient for present purposes.

Temperature and stress calculations were conducted by admitting temperature dependent material properties: thermal conductivity, specific heat, thermal expansion coefficient (Fig. 7) and elastic modulus (~400 GPa for both materials). Typical temperature distributions within the test specimen, determined both across the surface and through the

thickness, are plotted in Fig. 8. It is noted that there is an appreciable axial temperature gradient. Results for a thin disc can not, therefore, be expected to apply.

The time dependence of the maximum stress, at the center surface location, typically exhibits the form depicted in Fig. 9. It is observed that the peak stress develops at a time approximately coincident with the instant when the temperature at the disc periphery begins to diminish.

The procedure adopted for the calibration of the heat transfer coefficient involved calculations of the influence of h on the peak stress for Al_2O_3 at a specific temperature differential 575°C, pertinent to a 15N indentation precrack. The value of the heat transfer coefficient, h^*, that provided a peak tensile stress coincident with the biaxial fracture strength, for precracks of equivalent size (290 MPa), was then considered to be the correct value of h for that film temperature. A unique λ value for the test system was then deduced by inserting h^* into Eq. (3). The calibrated value of λ was employed for all subsequent stress calculations, yielding values of h that vary with temperature, through the temperature dependence of k_f and η_f (for the fluid medium).

Preliminary credence in the deduced value of h^* was established by comparing the measured failure times with estimates derived by analysis. For this purpose, it is noted that, since 10°C temperature

increments were used to determine the incidence of fracture, the experimental estimate of ΔT_c could exceed the actual value by < 10°C. Stress levels developed at a 10°C temperature separation were thus calculated, and a lower bound on the failure time established from the time when the stress at the upper temperature attained the median failure stress (Fig. 9). The time of 12 s determined using this procedure is of the same order as the measured failure times.

A series of calculations were conducted for ΔT values within the vicinity of the values measured for each of the two materials. These calculations permitted relationships between ΔT and the peak stress $\hat{\sigma}$ to be deduced for each material within the pertinent ΔT range, as plotted in Fig. 10. Imposing the median biaxial failure stress for each precrack size (Fig. 4) then allowed the critical ΔT for each thermal shock test to be predicted.

The trends in thermal fracture predicted in this manner (Fig. 3) are remarkably consistent with the measured behavior. Of particular merit are the accurate predictions obtained for SiC, which fractures in a very different ΔT range than the calibration material (Al_2O_3), by virtue both of appreciable differences in k and α and of significant variations in K_c and h. It is also noted that superior predictions are obtained by excluding radiation from the lower surface of the specimen.

5. IMPLICATIONS

The close prediction of thermal shock failure from (surface crack dominated) biaxial strength measurements strongly supports the notion that thermal fracture can be uniquely related to the stress field produced by the temperature transient. Many thermal shock failures originate from surface cracks (because the thermal stress gradient encourages failure from near-surface located defects). The present validation of the thermal failure process for this important defect type should thus be of substantial merit for the prediction of thermal shock failure in ceramic components.

The calibration of the heat transfer conditions for the present test arrangement permits the apparatus to be used for the quantitative determination of thermal shock resistance for a range of ceramics. The comparison can be conducted on surfaces prepared in a manner analogous to that used for actual components, thereby averting the extraneous influence of specimen edges. (Also, the relative temperature invariance of the heat transfer coefficient permits a direct ranking of thermal shock resistance.) Such quantitative thermal shock tests would allow both the elucidation of the statistical character of fracture and would permit the magnitude of thermal (e.g., interrupted heat flow) sources of stress intensification pertinent to fracture from fabrication defects (voids, inclusions, etc.) to be evaluated.

For intrinsically thermal shock resistant materials (SiC, Si_3N_4), more severe heat transfer conditions than those presently employed would need to be devised, in order to induce fracture within the temperature

capabilities of the test system. This might be achieved by increasing the specimen dimensions or, more expediently, by increasing the conductivity and decreasing the viscosity of the fluid (see Eq. (3)). An appropriate choice of fluid might be helium.

Finally, it is observed that the heat transfer calibration procedure adopted in the present study could provide an unequivocal method for heat transfer calibration in actual systems. Specifically, a small precrack could be placed at the location of maximum stress. Then, the time at which fracture initiates from the precrack could be measured, during a test run. Thereafter, a combination of the failure time with the magnitude of the failure stress at the crack would permit the heat transfer coefficient to be determined by comparison with a series of thermal stress calculations.

ACKNOWLEDGEMENT

The authors express their appreciation for the financial support of this research provided by the Carborundum Co. (K.T.F. and M.D.H.) and by the Office of Naval Research (A.G.E.) under contract no. N0014-79-C-0159. This work was also supported by the Director, Office of Energy Research, Office of Basic Energy Sciences, Materials Science Division of the U.S. Department of Energy under Contract No. W-7405-ENG-48.

FIGURE CAPTIONS

Fig. 1 A schematic of the thermal stress test apparatus.

Fig. 2 Thermally shocked discs

(a) a substantially supercritical thermal shock that activates many surface cracks

(b) a slightly supercritical thermal shock activating a central precrack.

To enhance the cracks the samples were immersed in a dye penetrant and illuminated under ultra-violet light.

Fig. 3 The influence of indentation load upon the critical temperature for thermal fracture of Al_2O_3 and SiC. Also shown are the critical temperatures predicted by the stress analysis from the biaxial strength results.

Fig. 4 The influence of indentation load on the biaxial flexure strength of Al_2O_3 and SiC.

Fig. 5 The assignment of the four types of element used in the finite element analysis.

Fig. 6 The four meshes employed in the finite element calculations. Mesh c was employed for the majority of calculations.

Fig. 7 Temperature dependent material properties of Al_2O_3 and SiC

(a) thermal conductivity

(b) specific heat

(c) thermal expansion

Fig. 8 The axial and radial temperature distributions in an Al_2O_3 sample subject to a temperature differential of 575°C, obtained at two times, 8s and 32s.

Fig. 9 The variation of the maximum tensile stress with time for Al_2O_3 subject to several values of ΔT. Also shown is the construction for estimating the lower bound failure time.

Fig. 10 The variation of the peak tensile stress with ΔT for (a) Al_2O_3, (b) SiC. Essentially identical results obtain for Al_2O_3 both with and without radiation; but a significant disparity exists for SiC, as illustrated.

REFERENCES

(1) T. K. Gupta, Jnl. Amer. Ceram. Soc., 55 (1972), 249.

(2) S. S. Manson and R. W. Smith, Jnl. Amer. Ceram. Soc., 38 [1] 18-27 (1955).

(3) Yagawa, G. and Masukazu, I., ASTM Eleventh National Symposium on Fracture Mechanics. Virginia Polytechnic Institute and State University, June 12-14, 1978.

(4) See for example, R. W. Davidge and G. Tappin, Proc. Brit. Ceram. Soc., 66 (1967), 405.

(5) Hasselman, D. P. H., "Unifed Theory of Thermal Shock Fracture Initiation and Crack Propagation in Brittle Ceramics," Jnl. Amer. Ceram. Soc. 52[11] 600-604 (1969).

(6) Becher, P. F. et al, "Thermal Shock Resistance of Ceramics: Size and Geometry Effects in Quench Tests," Amer. Ceram. Soc. Bull. 59 [5] 542-545 (1980).

(7) Jaeger, J. C., "Thermal Stress in Cylinders," Philos. Mag. 36 [257] 418 (1963).

(8) Ferber, E. A. and R. L. Scorah, "Heat Transfer to Water Boiling Under Pressure," Trans. ASME, 369-384 (1948).

(9) Emery, A. F. and A. S. Kobayashi, "Transient Stress Intensity Factors and Edge and Corner Cracks in Quench Test Specimens," Jnl. Amer. Ceram. Soc. 63 [7-8] 410-415 (1980).

(10) Petrovic, J. J. et al, "Controlled Surface Flaws in Hot-Pressed Si_3N_4," Jnl. Amer. Ceram. Soc. 58 [3-4] 113-116 (1975).

(11) Wachtman, Jr., J. B. et al, "Biaxial Flexure Tests of Ceramic Substrates," J. Mat. 7 [2] 188-194 (1972).

(12) B. R. Lawn, A. G. Evans, D. B. Marshall, Jnl. Amer. Ceram. Soc., in press.

(13) Polivka, R. M. and Wilson, E. L., "Finite Element Analysis of Nonlinear Heat Transfer Problems," University of California Structural Engineering Laboratory Report No. SESM 76-2, June 1976.

(14) Wilson, E. L., "SOLID SAP, A Static Analysis Program for Three Dimensional Structures," University of California Structural Engineering Laboratory Report No. UC SESM 71-19, Sept. 1971.

(15) Holman, J. P., Heat Transfer 3rd Edition; p. 186, McGraw-Hill, Inc., New York, 1972.

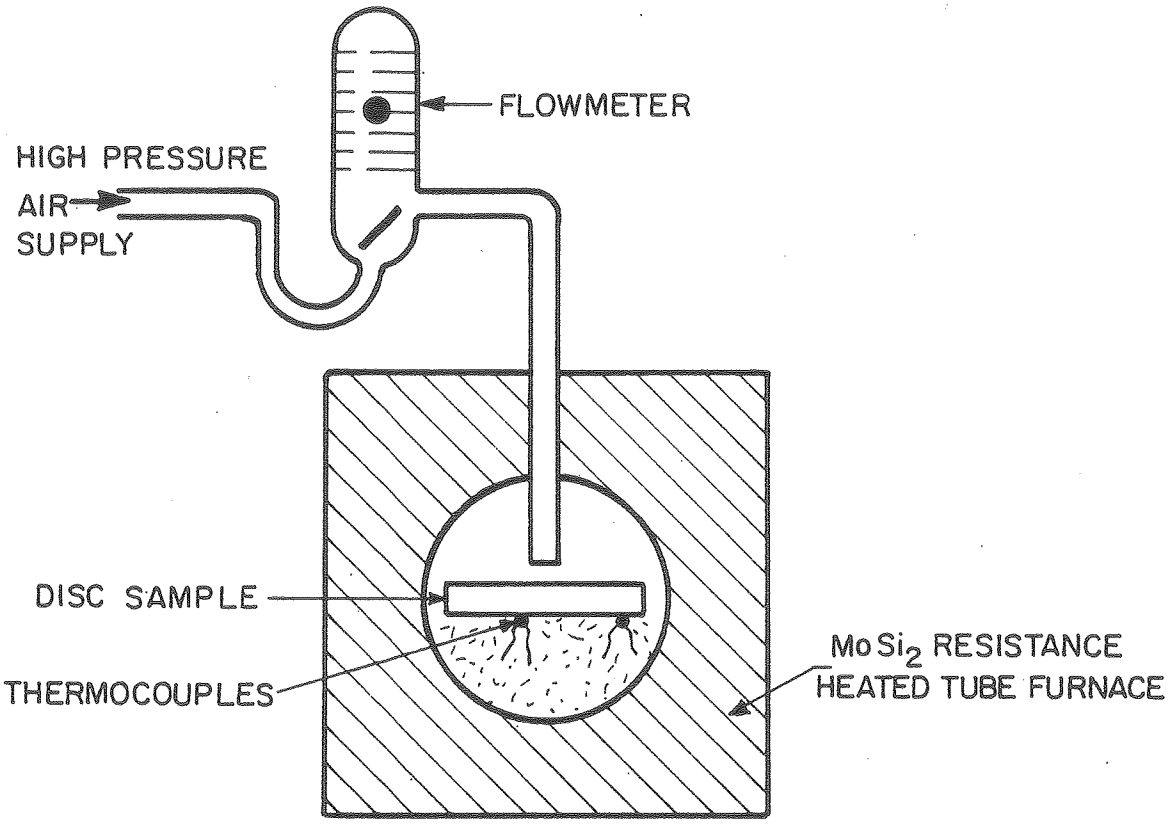
FLOWMETER
HIGH PRESSURE
AIR
SUPPLY
DISC SAMPLE
THERMOCOUPLES
$MoSi_2$ RESISTANCE
HEATED TUBE FURNACE
XBL 807-5569

Fig. 1

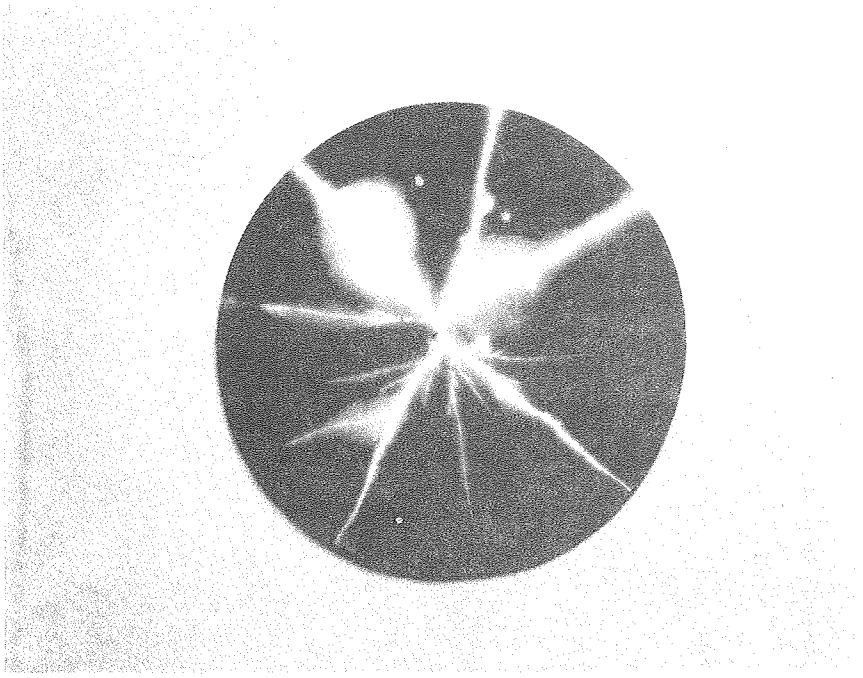

B

XBB808-9369

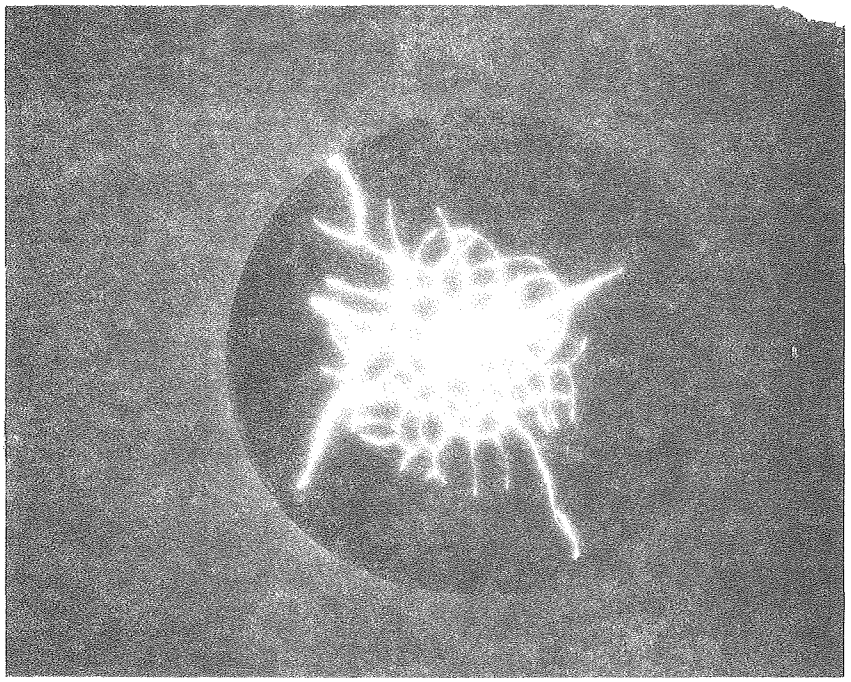

A

Fig. 2

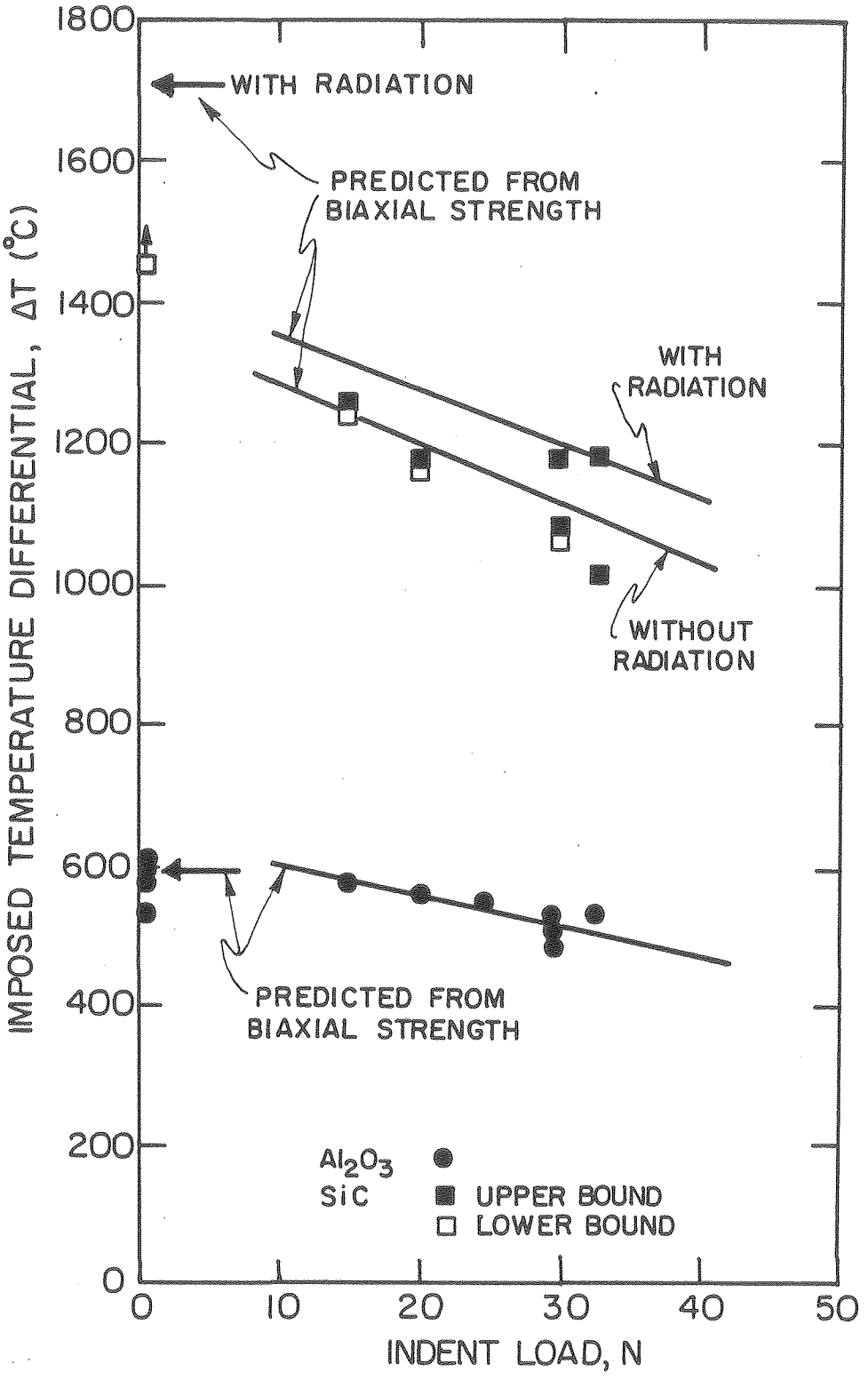
1800
1600
1400
1200
1000
800
600
400
200
0
IMPOSED TEMPERATURE DIFFERENTIAL, ΔT (°C)
WITH RADIATION
PREDICTED FROM BIAXIAL STRENGTH
WITH RADIATION
WITHOUT RADIATION
PREDICTED FROM BIAXIAL STRENGTH
Al2O3
SiC
UPPER BOUND
LOWER BOUND
0
10
20
30
40
50
INDENT LOAD, N
XBL 806-5291

Fig. 3

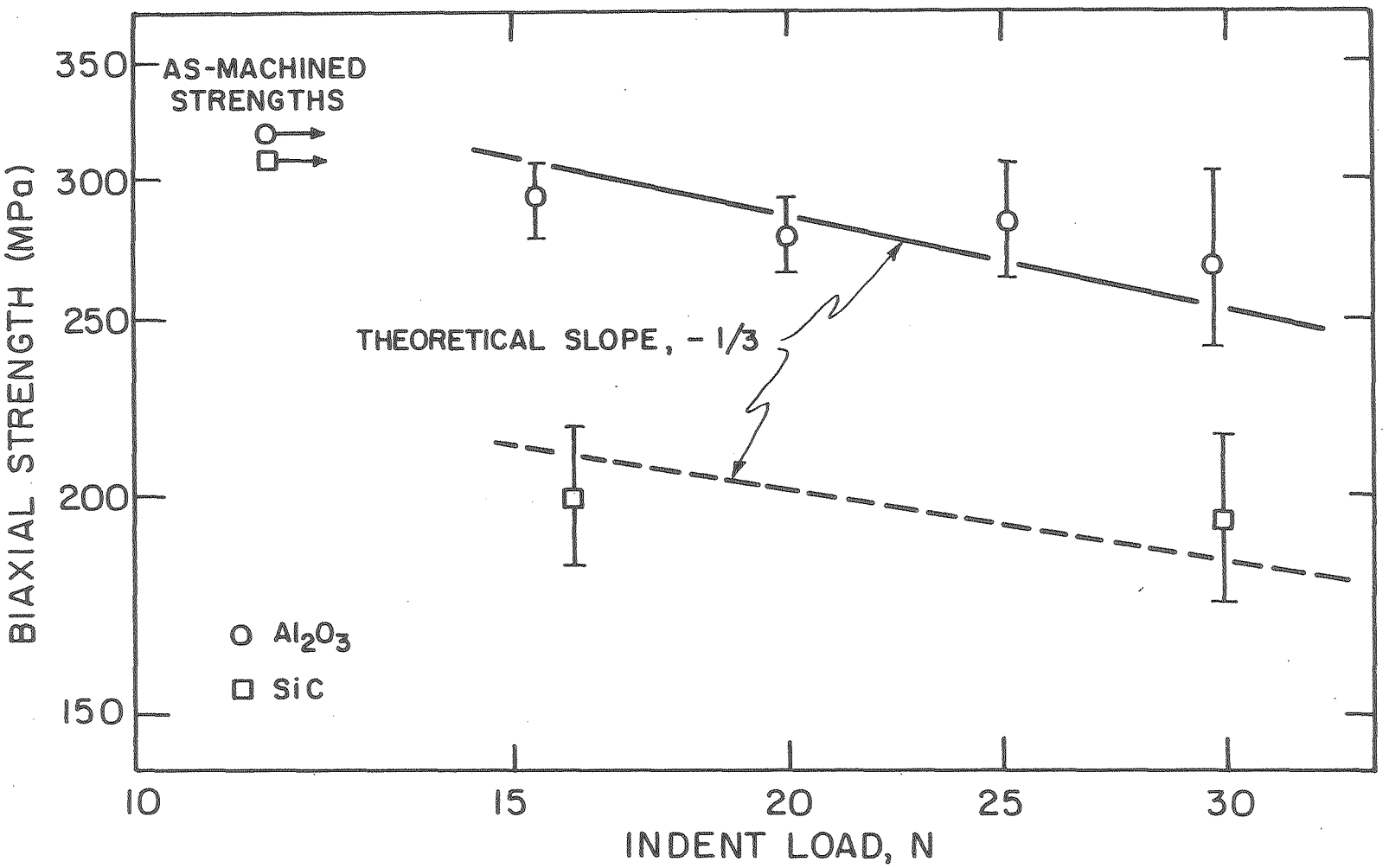
AS-MACHINED
STRENGTHS
THEORETICAL SLOPE, - 1/3
O Al_2O_3
□ SiC
BIAXIAL STRENGTH (MPa)
350
300
250
200
150
10
15
20
25
30
INDENT LOAD, N
XBL 806-5293

Fig. 4

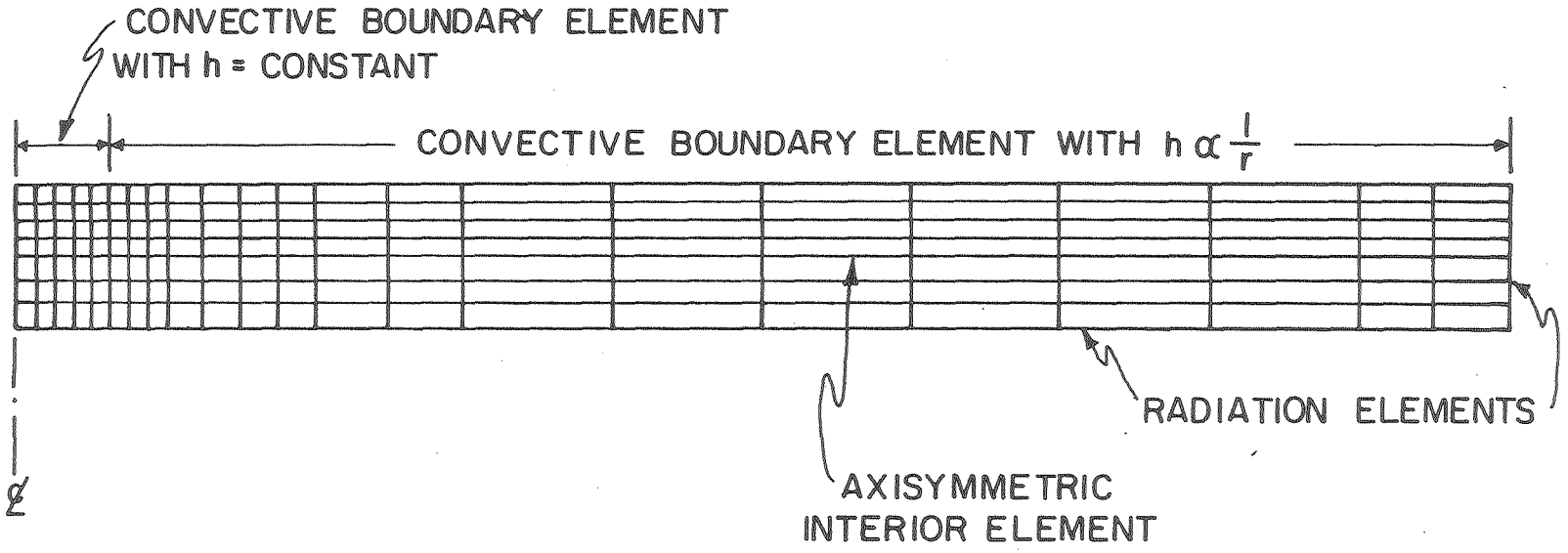

XBL 806-5292

Fig. 5

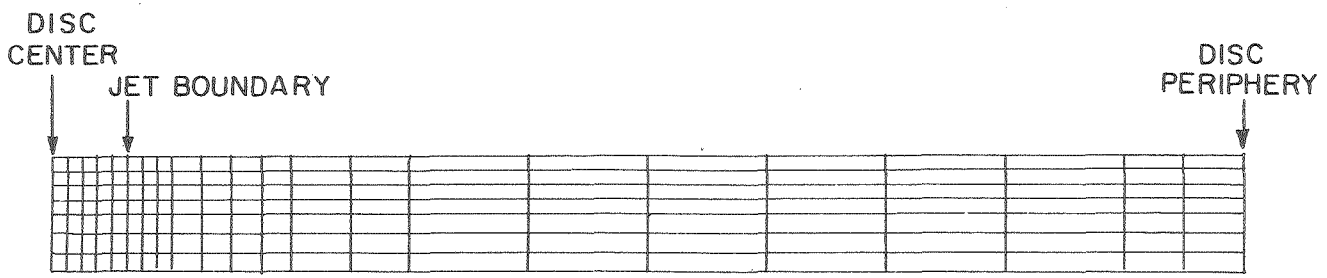

(a) 154 ELEMENT MESH: UNIFORM CENTRAL DISTRIBUTION

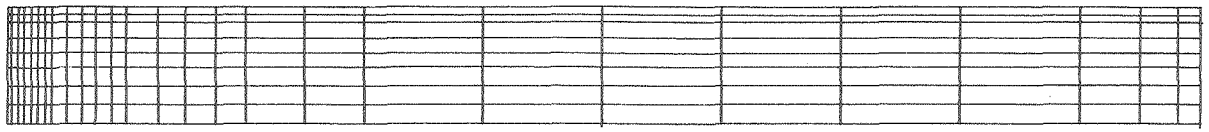

(b) 216 ELEMENT MESH: INHOMOGENEOUS CENTRAL DISTRIBUTION

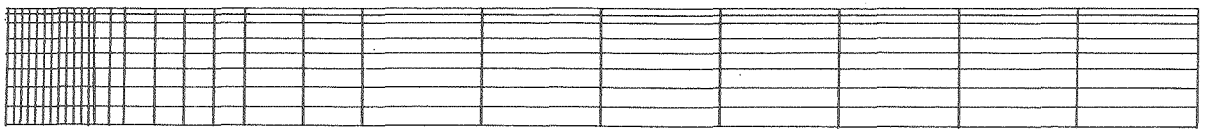

(c) 216 ELEMENT MESH: UNIFORM CENTRAL DISTRIBUTION

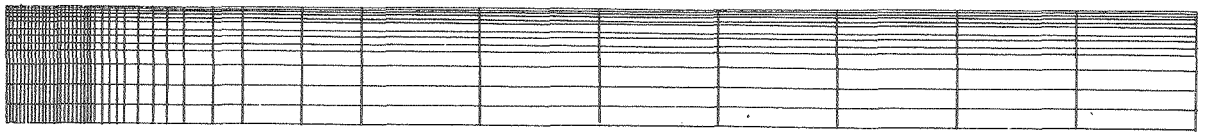

(d) 616 ELEMENT MESH

XBL 806-5297

Fig. 6

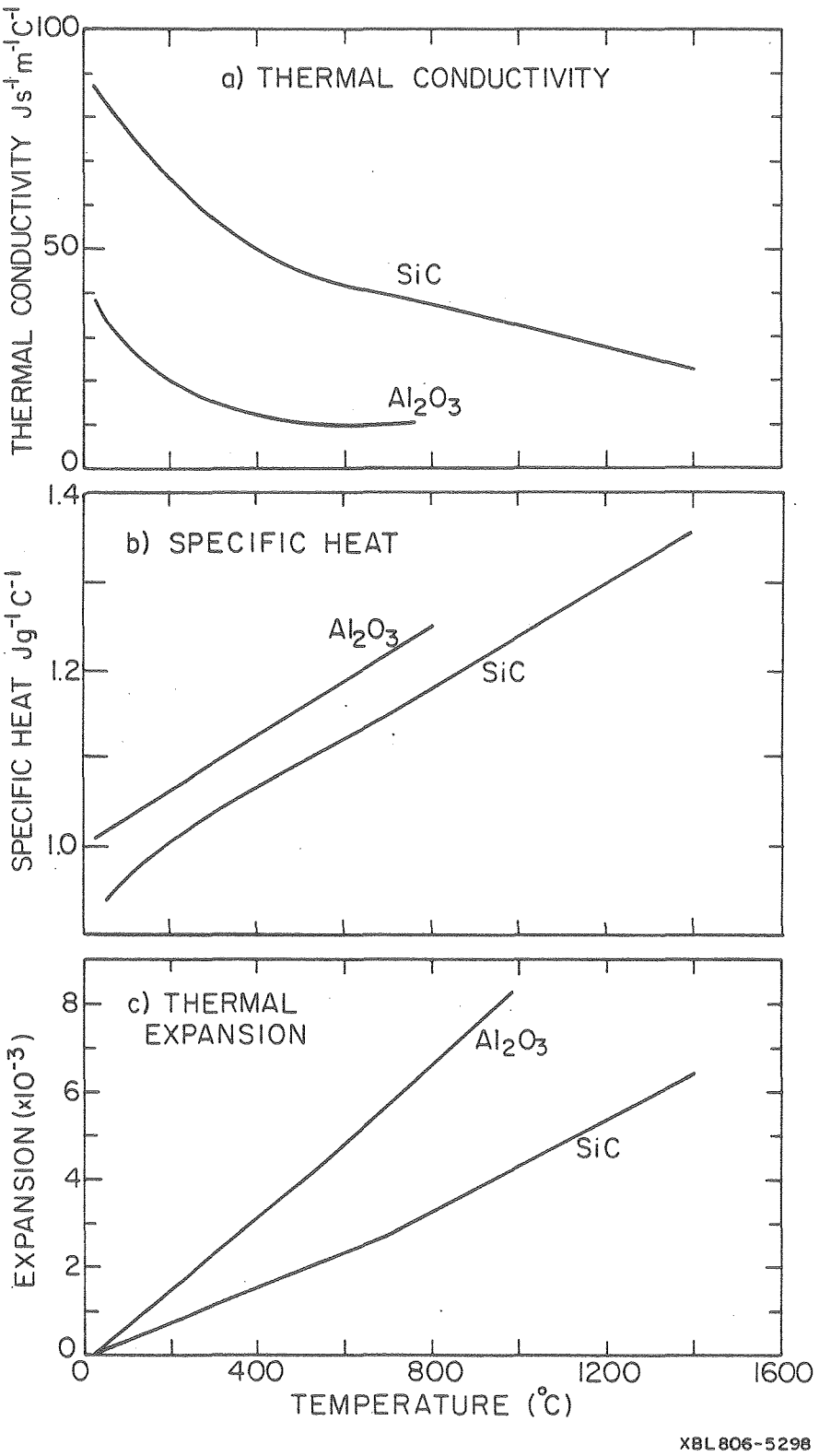
a) THERMAL CONDUCTIVITY
THERMAL CONDUCTIVITY Js⁻¹m⁻¹C⁻¹
100
50
0
SiC
Al2O3
b) SPECIFIC HEAT
SPECIFIC HEAT Jg⁻¹C⁻¹
1.4
1.2
1.0
Al2O3
SiC
c) THERMAL EXPANSION
EXPANSION (x10⁻³)
8
6
4
2
0
Al2O3
SiC
0
400
800
1200
1600
TEMPERATURE (°C)
XBL806-5298

Fig. 7

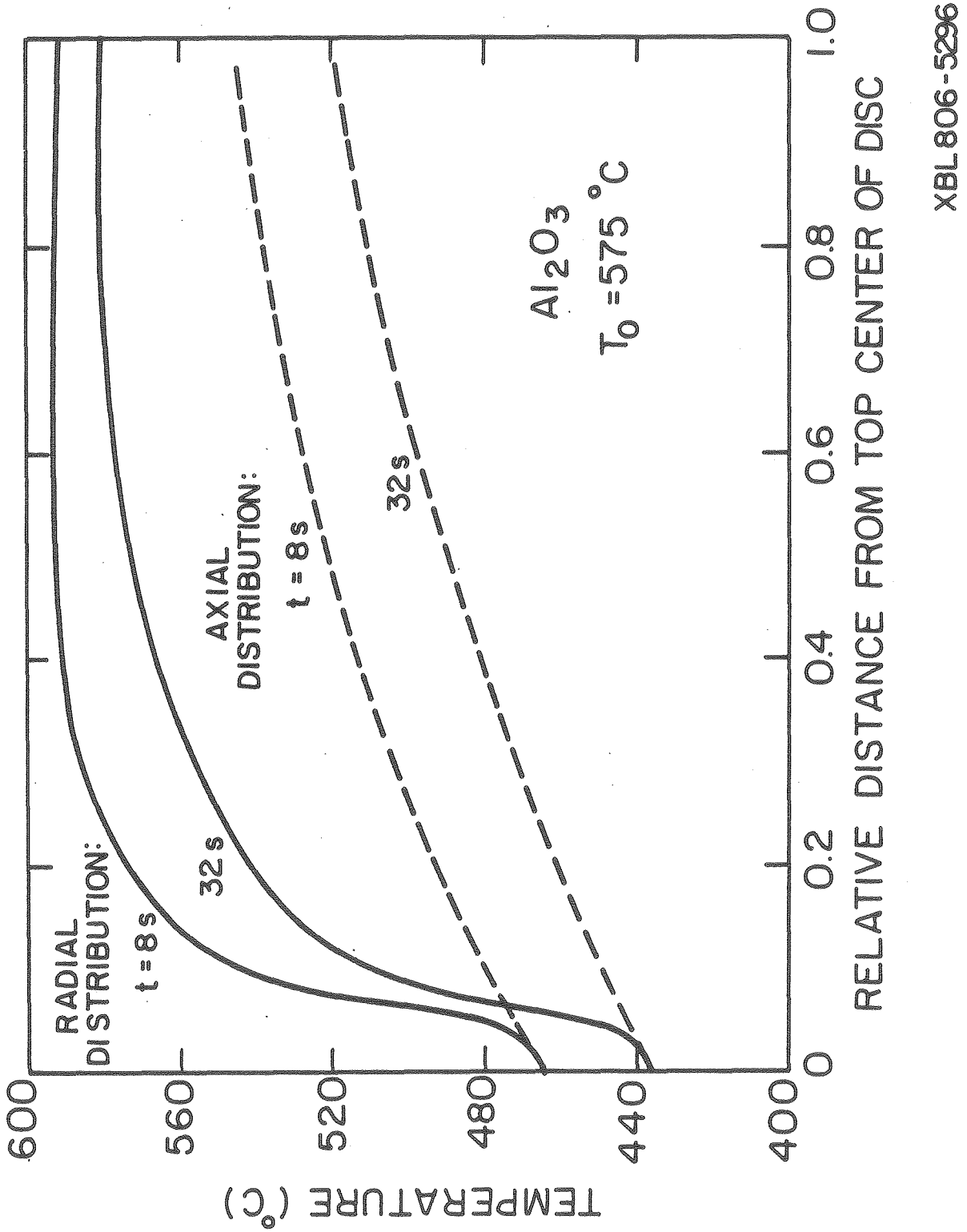
TEMPERATURE (°C)
600
560
520
480
440
400
0
0.2
0.4
0.6
0.8
1.0
RELATIVE DISTANCE FROM TOP CENTER OF DISC
RADIAL DISTRIBUTION: t = 8 s
32 s
AXIAL DISTRIBUTION: t = 8 s
32 s
Al2O3
T0 = 575 °C
XBL 806-5296

Fig. 8

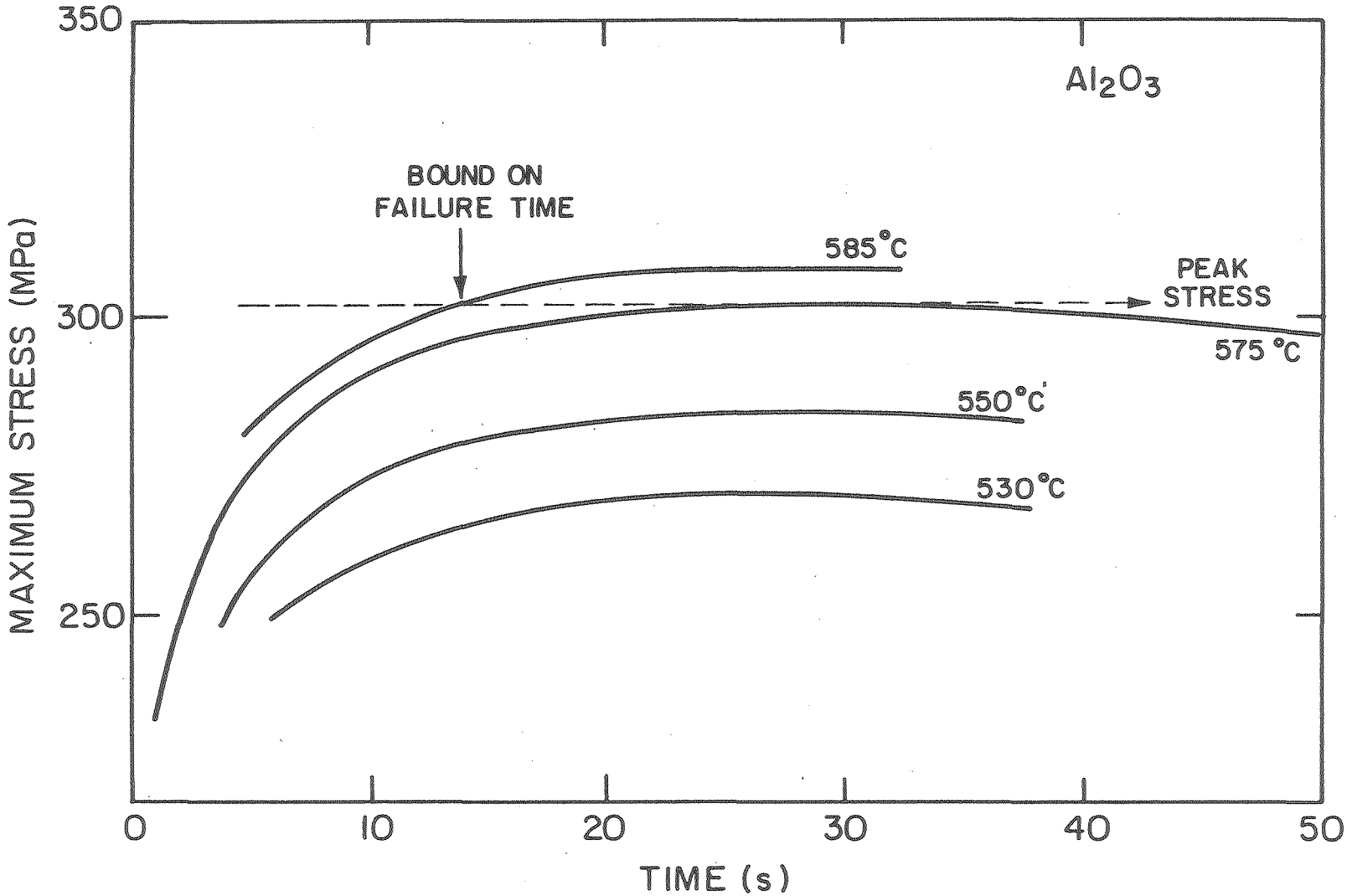
350
300
250
MAXIMUM STRESS (MPa)
Al_2O_3
BOUND ON
FAILURE TIME
585°C
PEAK
STRESS
575 °C
550°C
530°C
0
10
20
30
40
50
TIME (s)
XBL806-5295

Fig. 9

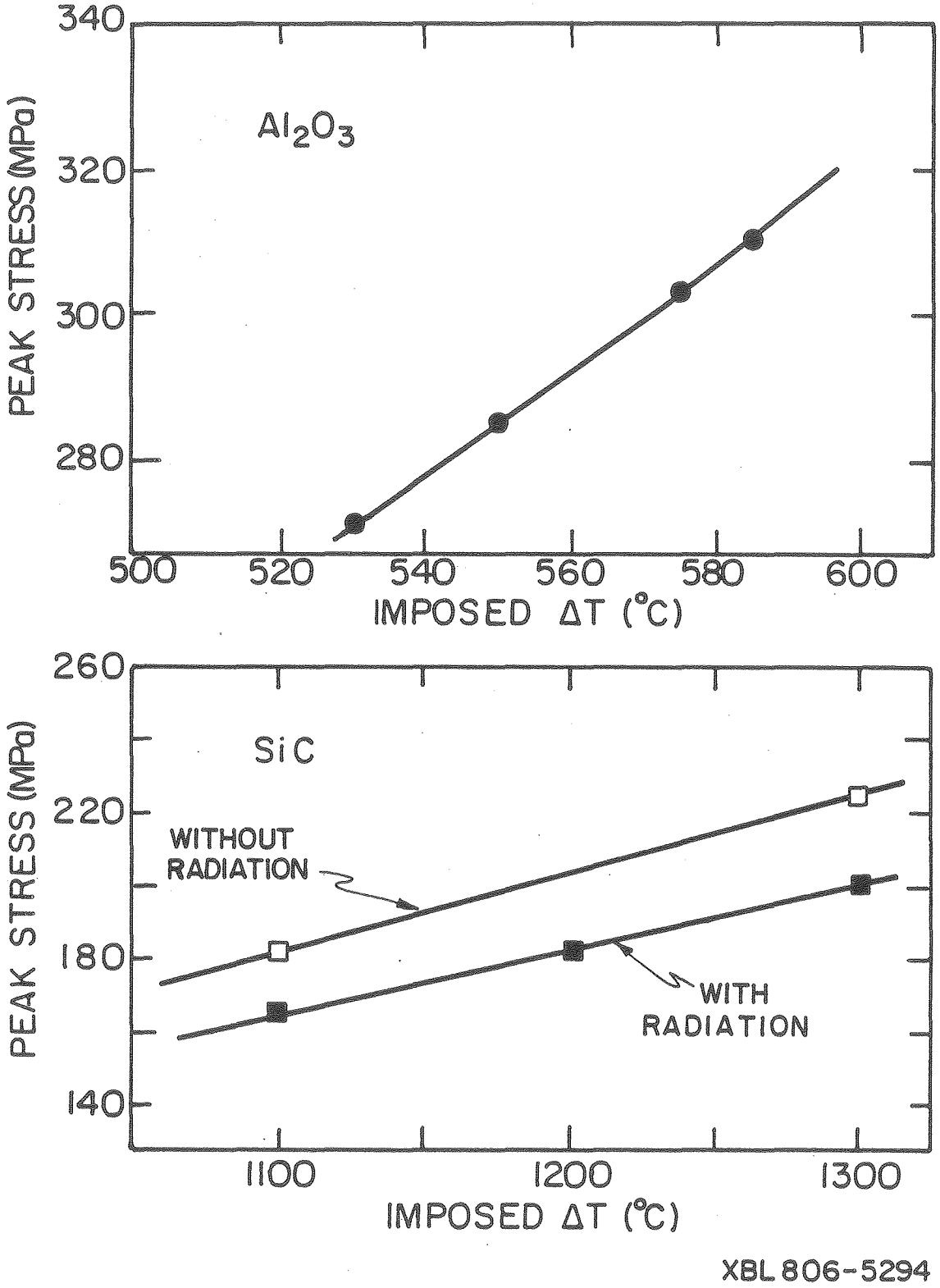
340
320
300
280
PEAK STRESS (MPa)
Al_2O_3
500
520
540
560
580
600
IMPOSED ΔT (°C)
260
220
180
140
PEAK STRESS (MPa)
SiC
WITHOUT RADIATION
WITH RADIATION
1100
1200
1300
IMPOSED ΔT (°C)
XBL 806-5294

Fig. 10